DOI:
10.1021/nn506164s

Document Version
Publisher's PDF, also known as Version of record

Blocking the Passage: C_{60} Geometrically Clogs K^+ Channels

Matteo Calvaresi,*,†,∥ Simone Furini,*,‡,∥ Carmen Domene,§,⊥ Andrea Bottoni,† and Francesco Zerbetto*,†

†Dipartimento di Chimica "G. Ciamician", Alma Mater Studiorum — Università di Bologna, via F. Selmi 2, 40126 Bologna, Italy, ‡Dipartimento di Biotecnologie Mediche, Università di Siena, viale M. Bracci 12, I-53100 Siena, Italy, §Chemistry Research Laboratory, University of Oxford, Oxford OX1 3TA, U.K., and ⊥Department of Chemistry, King's College London, Britannia House, 7 Trinity Street, London SE1 1DB, U.K. ∥M.C. and S.F. contributed equally.

ABSTRACT Classical molecular dynamics (MD) simulations combined with docking calculations, potential of mean force estimates with the umbrella sampling method, and molecular mechanic/Poisson—Boltzmann surface area (MM-PBSA) energy calculations reveal that C_{60} may block K^+ channels with two mechanisms: a low affinity blockage from the extracellular side, and an open-channel block from the intracellular side. The presence of a low affinity binding-site at the extracellular entrance of the channel is in agreement with the experimental results showing a fast and reversible block without use-dependence, from the extracellular compartment. Our simulation protocol suggests the existence of another binding site for C_{60} located in the channel cavity at the intracellular entrance of the selectivity filter. The escape barrier from this binding site is ∼21 kcal/mol making the corresponding kinetic rate of the order of minutes. The analysis of the change in solvent accessible surface area upon C_{60} binding shows that binding at this site is governed purely by shape complementarity, and that the molecular determinants of binding are conserved in the entire family of K^+ channels. The presence of this high-affinity binding site conserved among different K^+ channels may have serious implications for the toxicity of carbon nanomaterials.

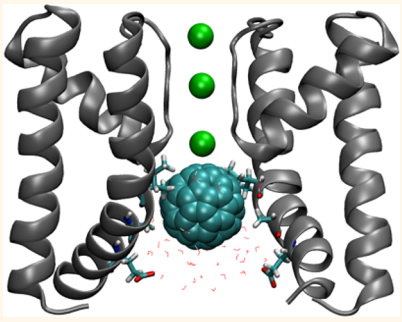

KEYWORDS: fullerene · K^+ channels · nanotoxicity · molecular dynamics · protein nanoparticle interaction

Biocomposites and hybrid biomaterials based on carbon nanoparticles (CNPs) satisfy many requisites of long-term biocompatibility and biological-level performance.[1−12] However, a toxicological profile of CNPs is emerging,[13−18] which also involves CNP interaction with proteins.[19−27] The design of new hybrids and the improvement of existing ones may depend crucially on the knowledge of the protein recognition pocket[28−31] for CNPs that can allow the design of new functionalization patterns of the CNPs[32−34] able to modulate their interaction with the protein.[19−31] K^+ channels represent one of the primary antitarget (*i.e.*, an unwanted target) in drug development and nanomedicine because their blockage causes potentially serious side effects. A growing list of pharmacological agents were restricted in their use, withdrawn from the market, or did not receive regulatory approval because of undesirable interactions with this class of membrane proteins.[35] K^+ channels regulate the fluxes of K^+ ions across cell membranes and govern a variety of functions that range from cardiac, skeletal, and muscle contraction to epithelial transport of nutrients and ions.[36,37] The pore domain of K^+ channels is made by four subunits symmetrically arranged around the permeation axis. Each subunit is characterized by the presence of two transmembrane helices (inner and outer helices). The region responsible for selective conduction of K^+ ions (selectivity filter) is located in the P-loop that links the outer and the inner helices. On the intracellular side of the selectivity filter, the pore opens into a water-filled cavity. In the closed-state of the channel, the inner helices close the intracellular entrance of the cavity. Instead in the open-state, the inner helices are bent and the intracellular entrance of the cavity is wide open. The architecture of the pore domain is conserved in all the experimental structures of K^+ channels known to date.[38−45] Park *et al.* found experimentally that C_{60} and carbon nanotubes can block ion channels,[46] with a fast and reversible mechanism without use-dependence. This behavior may be explained by CNPs binding at the extracellular entrance of the selectivity filter of K^+ channels.[46]

* Address correspondence to matteo.calvaresi3@unibo.it, simone.furini@unisi.it, francesco.zerbetto@unibo.it.

Received for review October 29, 2014 and accepted April 14, 2015.

Published online April 14, 2015
10.1021/nn506164s

In molecular dynamics (MD) simulations by Kraszewski *et al.*,[47] C_{60} molecules did not bind to the extracellular entrance of the selectivity filter. These MD simulations revealed alternative binding sites located at the protein−lipid interface, which may be responsible for impaired channel activity.[47] Kraszewski *et al.* considered also the possibility that C_{60}, because of its hydrophobicity, can pass the cellular membrane and block the channel from the intracellular side.[47] Indeed, when C_{60} was placed close to the intracellular entrance of the pore, it migrated toward the internal cavity. Subsequently, a large conformational change stabilized the binding.[47] Monticelli *et al.* explored an alternative explanation for the altered functioning of K^+ channels.[48] The authors tested the possibility that C_{60} alters the activity of ion channels through a lipid-mediated interaction. However, the simulations showed that the presence of C_{60} in the membrane interior has marginal effects on K^+ channel conformations.[48] Understanding the activity of C_{60} in K^+ channels requires the potential energy surface of the C_{60}-channel interactions. The large number of atoms of the system complicates its calculation. To overcome this hurdle, we combined classical MD simulations, docking calculations, potential of mean force (PMF) estimates with umbrella sampling, and molecular mechanic/Poisson−Boltzmann surface area (MM-PBSA) energy calculations.

RESULTS AND DISCUSSION

The atomic model of the channel was based on the experimental structure of the MthK protein, which corresponds to an open-state of the pore.[45] The channel was embedded in a pre-equilibrated bilayer of 160 1,2-dioleoyl-*sn*-glycero-3-phosphocholine (DOPC) molecules and the system was solvated by ~10.000 water molecules, 24 K^+ ions and 12 Cl^- ions were added. Three K^+ ions were placed in the selectivity filter together with two water molecules. After equilibration, an unrestrained MD trajectory of 100 ns was carried out (more details in the Methods section).

Blockage from the Extracellular Side. Experimental results by Park *et al.*,[46] imply the presence of an extracellular binding site for C_{60}. The free energy of a C_{60} molecule moving between the entrance of the selectivity filter and the extracellular compartment can provide quantitative information about the existence of this extracellular binding site. Umbrella sampling simulations were used to calculate the profile of the potential of mean force along a reaction coordinate, *z*, that describes the distance between the center of mass of the selectivity filter (backbone atoms of residues Thr59 to Gly63) and the center of mass of C_{60} (Figure 1).

C_{60} bound to the entrance of the selectivity filter is a local energy minimum. This minimum corresponds to the binding site proposed by Park and co-workers.[46] Its energy is ~4 kcal/mol higher than the energy of a

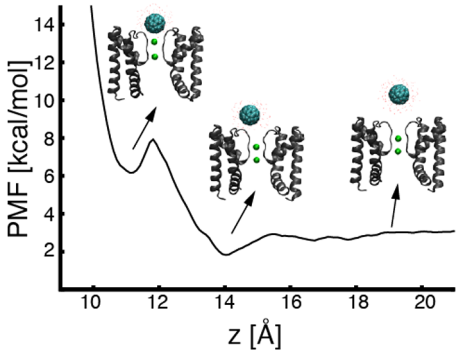

Figure 1. PMF for the movement of C_{60} from the extracellular entrance of the selectivity filter (located at z = 11 Å) to the extracellular compartment. Snapshots of representative configurations are shown using gray cartoons for two opposing subunits of the MthK channel, green spheres for K^+ ions in the selectivity filter, cyan spheres for C_{60}, red dots for water molecules closer than 6 Å to any atom of C_{60}.

C_{60} molecule in bulk solution. As a consequence, C_{60} is expected to block the MthK channel from this extracellular site only at high concentrations. A second minimum is also present, with C_{60} floating above the filter at a position where it can still interfere with ion conduction. These results agree with the dose-dependent blockage of the channel by carbon nanoparticles. The residues in the protein loops surrounding the extracellular entrance of the selectivity filter show a high variability among K^+ channels. Interactions of C_{60} with different sets of residues may increase or decrease the energy of these extracellular binding sites by a few kcal/mol, thus affecting the blocking affinity of C_{60} from the extracellular side. Experimentally it is observed that carbon nanoparticles inhibit EXP-2, KVS-1, human KCNQ1, Kv4.2, and HERG potassium channels to different extents.[46] The free energy profile calculated by umbrella sampling and the local energy minima for C_{60} near the extracellular entrance of the selectivity filter are also in agreement with the rapid off-rates and the fully reversible block observed experimentally.[46] In fact, washing the system during the measurements would allow the restoration of the full activity of the channel since C_{60} can easily unbind from the extracellular sites.

Blockage from the Intracellular Side. Docking calculations with a protocol able to recognize protein-CNPs interactions and structures sampled from the MD trajectory of the MthK channel, were used to define the initial structure of the C_{60}-MthK complex (more details in the Methods section).[23,24,49,50] The docking protocol suggests that the most favorable binding site for C_{60} in MthK is located in the intracellular cavity, in close proximity to the selectivity filter of the channel (Figure 2). Blockage from the intracellular site was previously proposed by Kraszewski *et al.*[47] However, in their MD simulations of MthK, C_{60} approaches the intracellular entrance of the channel, binds near the pore entrance (minimum z5 in Figure 3), and induces closure of the intracellular gate of the channel.

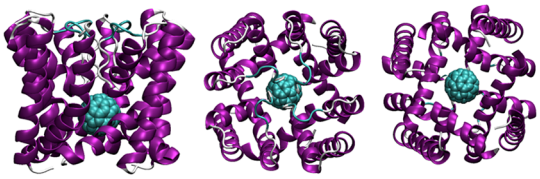

Figure 2. Docked complex. Left: front view. Middle: top view. Right: bottom view.

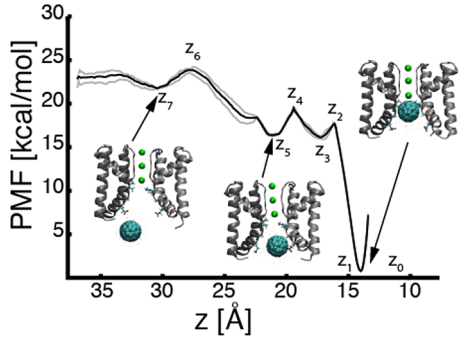

Figure 3. PMF for the displacement of C_{60} from the intracellular side of the selectivity filter (z = 14 Å) in the intracellular cavity of MthK to the intracellular solution. The black line illustrates the PMF computed using the full umbrella sampling trajectories; gray lines show the PMF computed using either the first or the second half of the umbrella sampling trajectories. Snapshots of representative configurations are shown using gray cartoons for two opposing subunits of the MthK channel, licorice representation for residues Ile84, Ala88 and Glu92 that face the intracellular cavity, green spheres for K^+ in the selectivity filter, cyan spheres for C_{60}, red dots for water molecules closer than 6 Å to any of the C_{60} atoms.

On the contrary in our docked structure C_{60} is located immediately below the selectivity filter (minimum z1 in Figure 3).

Interestingly, the docked structure was stable in a 100 ns MD trajectory, with an average deviation of C_{60} from the docked structure lower than 0.8 Å. The resolution of the protein structure was 1.45 Å. The small deviation observed in the dynamics validates *a posteriori* the use of the docking procedure to generate plausible structures. The radius at the intracellular gate was stable in our MD trajectory, and comparable to the value measured in an MD trajectory without C_{60} inside the cavity (Figure S1 in the Supporting Information). The PMF for the entrance of C_{60} into the intracellular cavity was calculated by umbrella sampling simulations, along the same reaction coordinate previously used to analyze C_{60}-blockage from the extracellular side. The region analyzed by umbrella sampling extended from the docked structure, z = 14 Å, to z = 30 Å, which corresponds to C_{60} in the intracellular solution (see Methods section for more details on the procedure).

The PMF presents four minima, separated by energy barriers that range from 1.6 to 3.1 kcal/mol (Table 1 and Figure 3). These barriers are easily overcome thermally. Once C_{60} is in the pore, the escape

TABLE 1. PMF: Energies and Characterization of the Points of Figure 3

	location z [Å]	energy [kcal/mol]	closest residues
z1	13.5	0	Ala88, Thr59, Ile84
z2	14.0	0.8	Ala88, Thr59, Ile84
z3	16.1	17.7	Ala88, Ile84, Gly85
z4	17.2	16.1	Ala88, Gly85, Ile84
z5	19.4	19.5	Ala88, Glu92, Gly85
z6	21.1	16.4	Ala88, Val89, Glu92
z7	27.9	23.9	Val18, Val89, Glu92
z8	30.5	21.8	Ala20, Val18, Arg93

barrier of ~21 kcal/mol makes the corresponding kinetic rate of the order of minutes (4×10^{-3} s^{-1}) at physiological temperature. The binding energy of C_{60} to the intracellular cavity is higher than the current estimates of the energy differences between C_{60} in water solution and in the lipid bilayer that was recently calculated in the 14–20 kcal mol^{-1} range.[51–55] Thus, thermodynamically this site is favored with respect to the embedding of C_{60} in the hydrophobic core of the membrane bilayer.

The experimental protocol used by Park *et al.* may explain why intracellular block of K^+ channels by C_{60} was not observed in their electrophysiological measurements.[46] In whole-cell experiments, C_{60} perfused from the extracellular side requires several minutes, if not hours, to enter into the cytoplasm.[56–59] On the time scale of the experiments performed by Park *et al.*, C_{60} does not have sufficient time to reach the binding site located in the intracellular cavity. Under these conditions, a high concentration of C_{60} molecules in the extracellular compartment can only populate the extracellular binding site of the selectivity filter. Microscopic techniques showed that on the hours time scale, C_{60} is taken up by cells and is distributed within the cytoplasm, in lysosomes, aligned along the plasma membrane and within the nucleus.[61–63] Fullerene molecules crosses the external cellular membrane and penetrates inside the cell following multiple energy-dependent pathways such as clathrin-mediated endocytosis, lipid-raft/caveolae-mediated endocytosis, and macropinocytosis.[56–60,60]

Carbon nanoparticles of a different nature, such as small diameter nanotubes, could be accommodated in the intracellular cavity in analogy to C_{60}. They could also establish further interactions with the intracellular sidewalls of the protein, which may provide a clogging activity with a higher energy escape barrier.

The mechanism of channel blocking appears to be governed by geometrical factors and to lack any other physical/chemical component that is usually required by conventional channel blockers. In other words, while the binding of conventional blockers to K^+ channels is governed by residue-specific interactions, the binding of C_{60} emerges from the complementarity between the

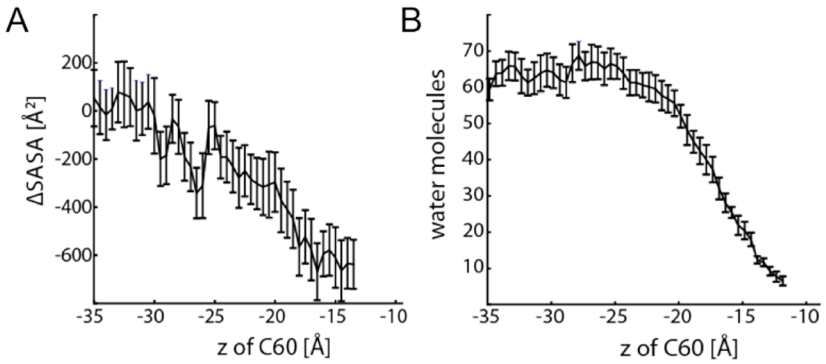

Figure 4. (A) Change in solvent accessible surface area (ΔSASA) upon C_{60} binding. (B) Water molecules inside the intracellular cavity. ΔSASA calculated as $SASA_{MthK+C60} - SASA_{MthK} - SASA_{C60}$, where $SASA_{MthK+C60}$, $SASA_{MthK}$ and $SASA_{C60}$ are the SASA of the complex, of isolated MthK and of C_{60}. A water molecule was considered inside the cavity when it was above the center of mass of residues Ile99 and below the center of mass of residues Thr59. Panels (A) and (B) were generated from the umbrella sampling trajectories used for the PMF calculations.

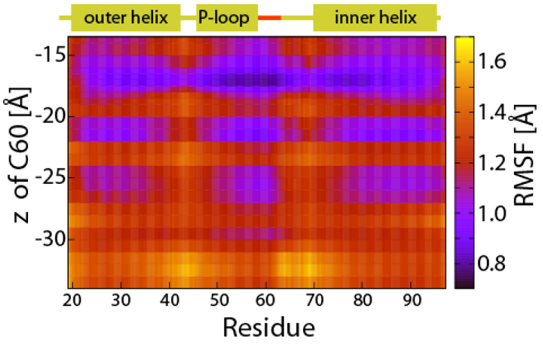

Figure 5. Root mean square fluctuations (RMSF) of the backbone atoms calculated from the average of the four protein chains. The structural elements of MthK are shown at the top. The red line after the P-loop corresponds to residues TVGYG of the selectivity filter.

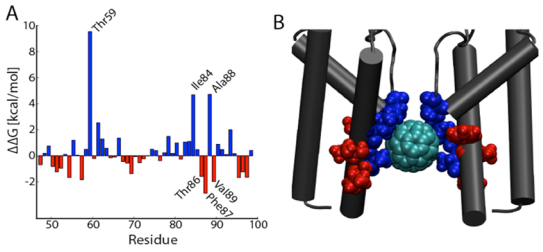

Figure 6. Contribution to the binding energy from protein residues as estimated by MM-PBSA calculations. (A) Change in binding energy (ΔΔ*G*) caused by the removal of the side chain atoms of the protein residues 47 to 99. (B) Snapshot from the MD trajectory of the MthK-C_{60} complex with residues Thr59, Ile84, and Ala88 in blue (residues with highest ΔΔ*G*); residues Thr86, Phe87, and Val89 in red (residues with lowest ΔΔ*G*); and C_{60} in cyan.

blocker and the intracellular cavity of the channel. Indeed, the analysis of the change in solvent accessible surface area (ΔSASA) upon C_{60} binding shows that binding is governed purely by shape complementarity (Figure 4), a phenomenon that resemble well-known encapsulation of pristine C_{60} molecules by macrocyclic receptors.[64]

C_{60} accommodates itself in the cavity, where it fits perfectly, and then it "picks up" whatever binding contributions it can from the residues forming the binding pocket. Another mechanism is also in operation. As hydrophobic C_{60} clogs the pore, it sheds water molecules (hydrophobic effect), as shown in Figure 4B. The complementary fit between C_{60} and the protein is evident also from the analysis of the root-mean-square fluctuations (RMSF) of the backbone atoms upon C_{60} binding (Figure 5). As C_{60} approaches its binding site, the fluctuations of the residues are reduced and the residues become glued to the fullerene cage. The phenomenon is particularly clear in the P-loop and in the selectivity filter, which are strongly stabilized by C_{60} binding. The energy of binding calculated by MM-PBSA was −29.2 kcal/mol (Table S1 in the Supporting Information), which is around 8 kcal/mol lower than the value estimated by umbrella sampling simulations. The entropic cost of binding is not included in the MM-PBSA calculations. Since the binding of C_{60} to the cavity causes a marked decrease in mobility (Figure 5), this approximation is likely responsible for the overestimate of the binding energy.

MM-PBSA can be used to estimate the net contribution of the individual amino acids to the binding energy (Figure 6). The residue contributing the most to the binding energy is threonine at the N-terminal of the selectivity filter (Thr59). This residue is conserved as threonine or serine in the entire K^+ channels family. Other residues that provide a favorable interaction with C_{60} are Ile84 and Ala88. Similar residues are found at these positions in all the voltage-gated K^+ channels (Ile or Val at position 84; Ala, Gly or Val at position 88).[65] The most important contribution to the binding energy arises from van der Waals interactions between these three amino acids and C_{60} (Table S1 in the Supporting Information). MM-PBSA also revealed the destabilizing effect on binding of some residue not exposed to the cavity, such as Thr86, Phe87 and Val89. The side chains of Thr86 and Val89 are directed toward the interior of the protein. The presence of C_{60} in the cavity forces these residues in strained configurations,

with an associated energy cost. Instead, Phe87 points to the cavity, and the destabilizing effect is due to the fact that upon C_{60} binding the hydroxyl group of Phe87 is no longer able to interact with water molecules in the intracellular cavity.

CONCLUSION

The atomistic simulations presented in this investigation suggest that C_{60} can block K^+ channels with two mechanisms: a fast reversible blockage from the extracellular side, in line with experimental results of Park *et al.*, and an energetically favored open-channel block from the intracellular side, never tested experimentally. The residues at the extracellular entrance of the channel, which mutate in different K^+ channels, may modify the binding energy to this site and modulate the affinity of extracellular blockage. On the contrary, the calculations show that binding of C_{60} to the intracellular site is governed purely by shape complementarity.

The presence of these two binding sites/mechanisms resembles the situation observed for quaternary ammonium pore blockers such as TEA.[66,67] TEA blocks K^+ channels both from the intracellular and the extracellular side, and the binding sites for intracellular and extracellular blockage coincide with those proposed here for C_{60}.[66,67] TEA blocks nearly every K^+-channel, when acting from the intracellular side, while blockage from the extracellular side is sensitive to the kind of channel considered and to mutations in the extracellular pore loops.[66,67] A similar mechanism can operate for C_{60}. Fullerene molecules can cross the external cellular membrane and penetrate inside the cell. According to our analyses, the intracellular binding site has an extremely high affinity for C_{60}. Moreover, this site is highly conserved in K^+ channels, which would make fullerene a potent nonselective blocker of K^+-channels. Experimental tests are needed to confirm the existence of this intracellular binding site. If C_{60} is trapped in the cavity upon closure of the intracellular gate, it can result in a use-dependent open-channel block. This cumulative and indiscriminate blockage of K^+ channels may have serious implications for the toxicity of carbon nanomaterials.

METHODS

Docking: The C_{60}-MthK Complex Structure Generation. The starting structures for the docking calculations were sampled from the MD trajectory of MthK with a period of 20 ns. These structures were screened for their potential binding to C_{60}. Docking models were obtained using the PatchDock algorithm.[68] PatchDock takes as input two molecules and computes three-dimensional transformations of one of the molecules with respect to the other with the aim of maximizing surface shape complementarity, while minimizing the number of steric clashes. Given a protein and a molecule, PatchDock (i) divides their surfaces into patches according to the surface shape (concave, convex, or flat), (ii) applies the geometric hashing algorithm to match concave patches with convex patches and flat patches with flat patches and generates a set of candidate transformations. (iii) Each candidate transformation is further evaluated by a set of scoring functions that estimate both the shape complementarity and the atomic desolvation energy of the complex.[69] Redundant solutions are discarded by use of rmsd (root-mean-square deviation) clustering. The algorithm implicitly addresses surface flexibility by allowing minor penetrations. Accurate rescoring of the complexes is then carried out using FireDock program.[70] This method simultaneously targets the problem of flexibility and scoring of solutions produced by fast rigid-body docking algorithms. Possible local readjustments of the protein structure are accounted for. Side-chain flexibility is modeled by rotamers and Monte Carlo minimization.[71] Following the rearrangement of the side-chains, the relative position of the docking partners is refined by Monte Carlo minimization of the binding score function. Desolvation free energy in the binding process is taken into account by a solvation model using estimated effective atomic contact energies (ACE).[69] All the candidates are ranked by the FireDock binding score,[52] and the structure with the highest value is retained as starting structure for the MD simulation of the C_{60}-MthK complex.

Molecular Dynamics Simulations. MD simulations were run for three atomic systems: the C_{60}-MthK complex, the MthK channel without C_{60}, and C_{60} alone. The latter system was simulated for 100 ns, after solvating C_{60} in ~600 water molecules. The atomic structure of MthK was based on the Protein Data Bank entry 3LDC.[45] Default protonation states were used for all ionizable residues. N- and C-terminals were methylamidated and acetylated, respectively. The channel was centered in the $x-y$ plane with the permeation axis aligned to the z-axis, and it was embedded in a pre-equilibrated bilayer of 160 DOPC molecules. The aromatic belt defined by the amphipathic residues Trp46 was aligned with the upper layer of the lipid membrane. Lipid molecules closer than 2.0 Å to protein atoms were removed. The system was solvated by ~10.000 water molecules, and 24 K^+ ions and 12 Cl^- ions were added. Three K^+ ions were manually placed in binding sites S4, S2 and S0 of the selectivity filter, while water molecules were placed in the remaining binding sites S3 and S1. In order to equilibrate the atoms around the channel, 10 000 steps of energy minimization and 400 ps of MD were performed, with harmonic restraints applied to protein backbone atoms and to the ions in the selectivity filter. An unrestrained MD trajectory of 100 ns followed. The minimal energy configuration identified by the docking analysis was used to define the starting structure to be used in MD simulation of the C_{60}-MthK complex. The complex C_{60}-MthK as identified by docking was superimposed on the last frame of the MD trajectory of MthK using the protein backbone atoms as reference. Then, the atomic coordinates of C_{60} in the model system of the C_{60}-MthK complex were defined as in the docking complex. Water molecules closer than 1.3 Å from C_{60} atoms were removed. Harmonic restraints were initially applied to C_{60} atoms and to protein backbone atoms, and gradually removed during a 1.5 ns period. Afterward, 100 ns of unrestrained MD were simulated. MD simulations were run using NAMD2.9,[72] and the CHARMM-27 all atom force field with CMAP correction.[73] The TIP3 model was used for water molecules.[74] Long-range electrostatic interactions were treated by the particle mesh Ewald algorithm,[75] with a maximum grid spacing of 1.0 Å. van der Waals interactions were gradually smoothed off at 10 Å (cutoff distance 12 Å). Langevin dynamics controlled the temperature at 300 K, and the Nosé–Hoover Langevin pressure control was used to keep a pressure of 1 bar.[76,77] Bonds with hydrogen atoms were restrained by the SETTLE algorithm,[78] in order to use a time step of 2 fs.

MM/PBSA Energy Calculations. The energy of binding, ΔG, was calculated as

$$\Delta G = G_{C60\text{-MthK}} - (G_{MthK} + G_{C60}) \quad (1)$$

where $G_{C60\text{-}MthK}$, G_{MthK}, and G_{C60} are respectively the free energies of the complex, the MthK channel, and the fullerene molecule. The energy of each molecular species was defined as the sum of the following terms:

$$G = E_{bond} + E_{vdw} + E_{elec} + G_{PB} + G_{SA} \quad (2)$$

In the former equation, E_{bond} is the contribution from the molecular mechanics bond energy, *i.e.*, sum of bond, angle, and dihedral energies; E_{vdw} is the molecular mechanics van der Waals energy contribution; E_{elec} is the molecular mechanics electrostatic energy; and G_{PB} and G_{SA} are polar and nonpolar contributions to the solvation energy. Polar and nonpolar contributions to the solvation energy were calculated using the APBS software.[79] The probe radius for the definition of the molecular surfaces was 1.4 Å. The relative dielectric constants were set to 80 and 2 respectively for the solvent and for the solutes. The nonpolar solvation energy was assumed proportional to the solvent accessible surface area, with proportionality constant equal to 0.0072 kcal mol^{-1} Å^{-2}. The triple-trajectory paradigm was adopted; *i.e.*, the energy terms were calculated using separate MD trajectories for the C_{60}-MthK complex, and for the isolated channel and C_{60}. The trajectories were sampled with a time lag of 1 ns. The contribution to the binding energy of the *i*-th residue was estimated as $\Delta\Delta Gi = \Delta Gi - \Delta G$, where ΔGi is the binding energy after the removal of the side chain atoms of residues *i* from the atomic structures of MthK and C_{60}-MthK. A positive value of $\Delta\Delta Gi$ corresponds to a residue that stabilizes the binding of C_{60} to the channel.

Umbrella Sampling. The umbrella sampling technique[80] was used to compute the potential of mean force (PMF) for the movement of C_{60} between the extracellular entrance of the selectivity filter and the extracellular compartment and between the intracellular cavity of MthK and the intracellular compartment. The distance along the *z*-axis between the center of mass of the selectivity filter (backbone atoms of residues 59 to 63) and the center of mass of C_{60} was used as reaction coordinate.

The starting configuration for the analysis of extracellular binding site was generated manually, placing the C_{60} molecule immediately above the selectivity filter, and removing K^+ ions and water molecules within 5 Å of C_{60} atoms. In order to equilibrate the surrounding atoms, 10 000 steps of energy minimization and 2 ns of MD were performed, with harmonic restraints applied to protein backbone atoms and to the ions in the selectivity filter. The initial configurations for the umbrella sampling simulations were generated by a steered MD simulation, with a harmonic restraint applied to the same reaction coordinate used for the umbrella sampling simulations (force constant equal to 10 kcal mol^{-1} Å^{-2}) that moved with constant velocity from 9.5 to 21.5 Å in the course of a 12 ns trajectory. The center of the harmonic restraint (force constant equal to 10 kcal mol^{-1} Å^{-2}) in umbrella sampling simulations moved in 1.0 Å steps between 9.5 and 21.5 Å, and a 2 ns trajectory was simulated for each restraining position. For each umbrella sampling simulation, the frame of the steered MD simulation with value of the reaction coordinate closer to the center of the harmonic potential was used as starting structure. The same protocol was used to estimate the PMF for intracellular blockage of MthK by C_{60}. The starting configuration for this calculation was the last frame of the unrestrained MD simulation of the C_{60}-MthK complex. The C_{60} molecule was moved from 14 Å, C_{60} immediately below the selectivity filter, to 30 Å, C_{60} in intracellular solution in a 16 ns steered MD simulation. Then, the same range of the reaction coordinate was analyzed by umbrella sampling simulations. Umbrella sampling that exhibited a drift in the value of the reaction coordinate were extended up to 8 ns. The cumulative simulations time for the two PMF calculations was 96 ns. Since the displacement of C_{60} in the $x-y$ plane is naturally bounded inside the channel but not in the extracellular solution, lateral movements of C_{60} were artificially confined by a biasing potential. The biasing potential was identically zero for C_{60} closer than 8 Å to the channel axis, while it increased harmonically with the distance from the axis outside this cylindrical region (force constant equal to 10 kcal mol^{-1} Å^{-2}). The unbiased PMF was computed using the weighted histogram analysis method.[81]

Conflict of Interest: The authors declare no competing financial interest.

Supporting Information Available: Radius at the intracellular entrance of the channel in simulations with C_{60} inside the cavity and without C_{60} and per-residue C_{60} binding energy. This material is available free of charge *via* the Internet at http://pubs.acs.org.

REFERENCES AND NOTES

1. Kostarelos, K.; Novoselov, K. S. Exploring the Interface of Graphene and Biology. *Science* **2014**, *344*, 261–263.
2. Calvaresi, M.; Zerbetto, F. The Devil and Holy Water: Protein and Carbon Nanotube Hybrids. *Acc. Chem. Res.* **2013**, *46*, 2454–2463.
3. Montellano, A.; Da Ros, T.; Bianco, A.; Prato, M. Fullerene C_{60} as a Multifunctional System for Drug and Gene Delivery. *Nanoscale* **2011**, *3*, 4035–4041.
4. Saito, N.; Haniu, H.; Usui, Y.; Aoki, K.; Hara, K.; Takanashi, S.; Shimizu, M.; Narita, N.; Okamoto, M.; Kobayashi, S.; *et al.* Safe Clinical Use of Carbon Nanotubes as Innovative Biomaterials. *Chem. Rev.* **2014**, *114*, 6040–6079.
5. Da Ros, T.; Prato, M. Medicinal Chemistry with Fullerenes and Fullerene Derivatives. *Chem. Commun.* **1999**, 663–669.
6. Heister, E.; Brunner, E. W.; Dieckmann, G. R.; Jurewicz, I.; Dalton, A. B. Are Carbon Nanotubes a Natural Solution? Applications in Biology and Medicine. *ACS Appl. Mater. Interfaces* **2013**, *5*, 1870–1891.
7. Kostarelos, K.; Bianco, A.; Prato, M. Promises, Facts and Challenges for Carbon Nanotubes in Imaging and Therapeutics. *Nat. Nanotechnol.* **2009**, *4*, 627–633.
8. Nakamura, E.; Isobe, H. Functionalized Fullerenes in Water. The First 10 Years of Their Chemistry, Biology, and Nanoscience. *Acc. Chem. Res.* **2003**, *36*, 807–815.
9. Cha, C.; Ryon Shin, S.; Annabi, N.; Dokmeci, M. R.; Khademhosseini, A. Carbon-Based Nanomaterials: Multifunctional Materials for Biomedical Engineering. *ACS Nano* **2013**, *7*, 2891–2897.
10. Nakanishi, W.; Minami, K.; Shrestha, L. K.; Ji, Q.; Hill, J. P.; Ariga, K. Bioactive Nanocarbon Assemblies: Nanoarchitectonics and Applications. *Nano Today* **2014**, *9*, 378–394.
11. Chen, Z.; Mao, R.; Liu, Y. Fullerenes for Cancer Diagnosis and Therapy: Preparation, Biological and Clinical Perspectives. *Curr. Drug Metab.* **2012**, *13*, 1035–1045.
12. Baati, T.; Bourasset, F.; Gharbi, N.; Njim, L.; Abderrabba, M.; Kerkeni, A.; Szwarc, H.; Moussa, F. The Prolongation of the Lifespan of Rats by Repeated Oral Administration of [60] Fullerene. *Biomaterials* **2012**, *33*, 6292–6294.
13. Kagan, V. E.; Bayir, H.; Shvedova, A. A. Nanomedicine and Nanotoxicology: Two Sides of the Same Coin. *Nanomedicine* **2005**, *1*, 313–316.
14. Krug, H. F.; Wick, P. Nanotoxicology: An Interdisciplinary Challenge. *Angew. Chem., Int. Ed.* **2011**, *50*, 1260–1278.
15. Jia, G.; Wang, H.; Yan, L.; Wang, X.; Pei, R.; Yan, T.; Zhao, Y.; Guo, X. Cytotoxicity of Carbon Nanomaterials: Single-Wall Nanotube, Multi-Wall Nanotube, and Fullerene. *Environ. Sci. Technol.* **2005**, *39*, 1378–1383.
16. Bussy, C.; Ali-Boucetta, H.; Kostarelos, K. Safety Considerations for Graphene: Lessons Learnt from Carbon Nanotubes. *Acc. Chem. Res.* **2013**, *46*, 692–701.
17. Bianco, A. Graphene: Safe or Toxic? The Two Faces of the Medal. *Angew. Chem., Int. Ed.* **2013**, *52*, 4986–4997.
18. Dallavalle, M.; Calvaresi, M.; Bottoni, A.; Melle-Franco, M.; Zerbetto, F. Graphene Can Wreak Havoc with Cell Membranes. *ACS Appl. Mater. Interfaces* **2015**, *7*, 4406–4414.
19. Zuo, G.; Kang, S.-G.; Xiu, P.; Zhao, Y.; Zhou, R. Interactions Between Proteins and Carbon-Based Nanoparticles: Exploring the Origin of Nanotoxicity at the Molecular Level. *Small* **2013**, *9*, 1546–1556.
20. Yang, S.-T.; Liu, Y.; Wang, Y.-W.; Cao, A. Biosafety and Bioapplication of Nanomaterials by Designing Protein-Nanoparticle Interactions. *Small* **2013**, *9*, 1635–1653.

21. Zuo, G.; Huang, Q.; Wei, G.; Zhou, R.; Fang, H. Plugging into Proteins: Poisoning Protein Function by a Hydrophobic Nanoparticle. *ACS Nano* **2010**, *4*, 7508–7514.
22. Turabekova, M.; Rasulev, B.; Theodore, M.; Jackman, J.; Leszczynska, D.; Leszczynski, J. Immunotoxicity of Nanoparticles: A Computational Study Suggests that CNTs and C_{60} Fullerenes Might Be Recognized as Pathogens by Toll-like Receptors. *Nanoscale* **2014**, *6*, 3488–3495.
23. Calvaresi, M.; Zerbetto, F. Baiting Proteins with C_{60}. *ACS Nano* **2010**, *4*, 2283–2299.
24. Calvaresi, M.; Arnesano, F.; Bonacchi, S.; Bottoni, A.; Calò, V.; Conte, S.; Falini, G.; Fermani, S.; Losacco, M.; Montalti, M.; *et al.* C_{60}@Lysozyme: Direct Observation by Nuclear Magnetic Resonance of a 1:1 Fullerene Protein Adduct. *ACS Nano* **2014**, *8*, 1871–1877.
25. Ge, C.; Du, J.; Zhao, L.; Wang, L.; Liu, Y.; Li, D.; Yang, Y.; Zhou, R.; Zhao, Y.; Chai, Z.; *et al.* Binding of Blood Proteins to Carbon Nanotubes Reduces Cytotoxicity. *Proc. Natl. Acad. Sci. U. S. A.* **2011**, *108*, 16968–16973.
26. Yanamala, N.; Kagan, V. E.; Shvedova, A. A. Molecular Modeling in Structural Nano-Toxicology: Interactions of Nano-Particles with Nano-Machinery of Cells. *Adv. Drug Delivery Rev.* **2013**, *65*, 2070–2077.
27. Ratnikova, T. A.; Govindan, P. N.; Salonen, E.; Ke, P. C. *In Vitro* Polymerization of Microtubules with a Fullerene Derivative. *ACS Nano* **2011**, *5*, 6306–6314.
28. Miao, Y.; Xu, J.; Shen, Y.; Chen, L.; Bian, Y.; Hu, Y.; Zhou, W.; Zheng, F.; Man, N.; Shen, Y.; *et al.* Nanoparticle as Signaling Protein Mimic: Robust Structural and Functional Modulation of CaMKII upon Specific Binding to Fullerene C60 Nanocrystals. *ACS Nano* **2014**, *8*, 6131–6144.
29. Yang, Z.; Kang, S.; Zhou, R. Nanomedicine: *De Novo* Design of Nanodrugs. *Nanoscale* **2014**, *6*, 663–677.
30. Durdagi, S.; Supuran, C. T.; Strom, T. A.; Doostdar, N.; Kumar, M. K.; Barron, A. R.; Mavromoustakos, T.; Papadopoulos, M. G. *In Silico* Drug Screening Approach for the Design of Magic Bullets: A Successful Example with Anti-HIV Fullerene Derivatized Amino Acids. *J. Chem. Inf. Model.* **2009**, *49*, 1139–1143.
31. Mentovich, E.; Belgorodsky, B.; Gozin, M.; Richter, S.; Cohen, H. Doped Biomolecules in Miniaturized Electric Junctions. *J. Am. Chem. Soc.* **2012**, *134*, 8468–8473.
32. Bianco, A.; Kostarelos, K.; Prato, M. Making Carbon Nanotubes Biocompatible and Biodegradable. *Chem. Commun.* **2011**, *47*, 10182–10188.
33. Ali-Boucetta, H.; Nunes, A.; Sainz, R.; Herrero, M. A.; Tian, B.; Prato, M.; Bianco, A.; Kostarelos, K. Asbestos-Like Pathogenicity of Long Carbon Nanotubes Alleviated by Chemical Functionalization. *Angew. Chem., Int. Ed.* **2013**, *52*, 2274–2278.
34. Radic, S.; Nedumpully-Govindan, P.; Chen, R.; Salonen, E.; Brown, J. M.; Ke, P. K.; Ding, F. Effect of Fullerenol Surface Chemistry on Nanoparticle Binding-Induced Protein Misfolding. *Nanoscale* **2014**, *6*, 8340–8349.
35. Raschi, E.; Vasina, V.; Poluzzi, E.; De Ponti, F. The hERG K^+ Channel: Target and Antitarget Strategies in Drug Development. *Pharmacol. Res.* **2008**, *57*, 181–195.
36. Hille, B. *Ionic Channels of Excitable Membranes*, 3rd ed.; Sinauer Associates Inc.: Sunderland, MA, 2001.
37. Ashcroft, F. M. *Ion Channels and Disease*; Academic Press: San Diego, CA, 2000.
38. Doyle, D. A.; Cabral, J. M.; Pfuetzner, R. A.; Kuo, A.; Gulbis, J. M.; Cohen, S. L.; Chait, B. T.; MacKinnon, R. The Structure of the Potassium Channel: Molecular Basis of K^+ Conduction and Selectivity. *Science* **1998**, *280*, 69–77.
39. Jiang, Y.; Lee, A.; Chen, J.; Cadene, M.; Chait, B. T.; MacKinnon, R. The Open Pore Conformation of Potassium Channels. *Nature* **2002**, *417*, 515–522.
40. Kuo, A.; Gulbis, J. M.; Antcliff, J. F.; Rahman, T.; Lowe, E. D.; Zimmer, J.; Cuthbertson, J.; Ashcroft, F. M.; Ezaki, T.; Doyle, D. A. Crystal Structure of the Potassium Channel KirBac1.1 in the Closed State. *Science* **2003**, *300*, 1922–1926.
41. Jiang, Y.; Lee, A.; Chen, J.; Ruta, V.; Cadene, M.; Chait, B. T.; MacKinnon, R. X-ray Structure of a Voltage-Dependent K^+ Channel. *Nature* **2003**, *423*, 33–41.
42. Long, S. B.; Campbell, E. B.; MacKinnon, R. Crystal Structure of a Mammalian Voltage-Dependent Shaker Family K^+ Channel. *Science* **2005**, *309*, 897–903.
43. Brohawn, S. G.; del Marmol, J.; MacKinnon, R. Crystal Structure of the Human K2P TRAAK, a Lipid- and Mechano-Sensitive K^+ Ion Channel. *Science* **2012**, *335*, 436–441.
44. Miller, A. N.; Long, S. B. Crystal Structure of the Human Two-Pore Domain Potassium Channel K2P1. *Science* **2012**, *335*, 432–436.
45. Ye, S.; Li, Y.; Jiang, Y. Novel Insights into K^+ Selectivity from High-Resolution Structures of an Open K^+ Channel Pore. *Nat. Struct. Mol. Biol.* **2010**, *17*, 1019–1023.
46. Park, K. H.; Chhowalla, M.; Iqbal, Z.; Sesti, F. Single-Walled Carbon Nanotubes are a New Class of Ion Channel Blockers. *J. Biol. Chem.* **2003**, *278*, 50212–50216.
47. Kraszewski, S.; Tarek, M.; Treptow, W.; Ramseyer, C. Affinity of C_{60} Neat Fullerenes with Membrane Proteins: A Computational Study on Potassium Channels. *ACS Nano* **2010**, *4*, 4158–4164.
48. Monticelli, L.; Barnoud, J.; Orlowskid, A.; Vattulainen, I. Interaction of C_{70} Fullerene with the Kv1.2 Potassium Channel. *Phys. Chem. Chem. Phys.* **2012**, *14*, 12526–12533.
49. Calvaresi, M.; Zerbetto, F. Fullerene Sorting Proteins. *Nanoscale* **2011**, *3*, 2873–2881.
50. Calvaresi, M.; Hoefinger, S.; Zerbetto, F. Probing the Structure of Lysozyme-Carbon Nanotube Hybrids with Molecular Dynamics. *Chem.—Eur. J.* **2012**, *18*, 4308–4313.
51. Qiao, R.; Roberts, A. P.; Mount, A. S.; Klaine, S. J.; Ke, P. C. Translocation of C_{60} and its Derivatives Across a Lipid Bilayer. *Nano Lett.* **2007**, *7*, 614–619.
52. Bedrov, D.; Smith, G. D.; Davande, H.; Li, L. Passive Transport of C_{60} Fullerenes Through a Lipid Membrane: A Molecular Dynamics Simulation Study. *J. Phys. Chem. B* **2008**, *112*, 2078–2084.
53. Fiedler, S. L.; Violi, A. Simulation of Nanoparticle Permeation Through a Lipid Membrane. *Biophys. J.* **2010**, *99*, 144–152.
54. Höfinger, S.; Melle-Franco, M.; Gallo, T.; Cantelli, A.; Calvaresi, M.; Gomes, J. A. N. F.; Zerbetto, F. A Computational Analysis of the Insertion of Carbon Nanotubes into Cellular Membranes. *Biomaterials* **2011**, *32*, 7079–7085.
55. Bozdaganyan, M. E.; Orekhov, P. S.; Shaytan, A. K.; Shaitan, K. V. Comparative Computational Study of Interaction of C_{60}-Fullerene and Tris-Malonyl-C_{60}-Fullerene Isomers with Lipid Bilayer: Relation to Their Antioxidant Effect. *PLoS One* **2014**, *9*, e102487.
56. Salonen, E.; Lin, S.; Reid, M. L.; Allegood, M.; Wang, X.; Rao, A. M.; Vattulainen, I.; Ke, P. C. Real-Time Translocation of Fullerene Reveals Cell Contraction. *Small* **2008**, *4*, 1986–1992.
57. Raoof, M.; Mackeyev, Y.; Cheney, M. A.; Wilson, L. J.; Curley, S. A. Internalization of C60 Fullerenes into Cancer Cells with Accumulation in the Nucleus *via* the Nuclear Pore Complex. *Biomaterials* **2012**, *33*, 2952–2960.
58. Lucafò, M.; Pacor, S.; Fabbro, C.; Da Ros, T.; Zorzet, S.; Prato, M.; Sava, G. Study of a Potential Drug Delivery System Based on Carbon Nanoparticles: Effects of Fullerene Derivatives in MCF7Mammary Carcinoma Cells. *J. Nanopart. Res.* **2012**, *14*, 830.
59. Dellinger, A.; Zhou, Z.; Norton, S. K.; Lenk, R.; Conrad, D.; Kepley, C. L. Uptake and Distribution of Fullerenes in Human Mast Cells. *Nanomedicine* **2010**, *6*, 575–582.
60. Foley, S.; Crowley, C.; Smaihi, M.; Bonfils, C.; Erlanger, B. F.; Seta, P.; Larroque, C. Cellular Localisation of a Water-Soluble Fullerene Derivative. *Biochem. Biophys. Res. Commun.* **2002**, *294*, 116–119.
61. Porter, A. E.; Muller, K.; Skepper, J.; Midgley, P.; Welland, M. Uptake of C_{60} by Human Monocyte Macrophages, its Localization and Implications for Toxicity: Studied by High Resolution Electron Microscopy and Electron Tomography. *Acta Biomater.* **2006**, *2*, 409–419.
62. Levi, N.; Hantgan, R. R.; Lively, M. O.; Carroll, D. L.; Prasad, G. L. C_{60}-Fullerenes: Detection of Intracellular Photoluminescence and Lack of Cytotoxic Effects. *J. Nanobiotechnol.* **2006**, *4*, 14.

63. Porter, A. E.; Gass, M.; Muller, K.; Skepper, J. N.; Midgley, P.; Welland, M. Visualizing the Uptake of C_{60} to the Cytoplasm and Nucleus of Human Monocyte-Derived Macrophage Cells Using Energy-Filtered Transmission Electron Microscopy and Electron Tomography. *Environ. Sci. Technol.* **2007**, *41*, 3012–3017.
64. Canevet, D.; Pérez, E. M.; Martín, N. Wraparound Hosts for Fullerenes: Tailored Macrocycles and Cages. *Angew. Chem., Int. Ed.* **2011**, *50*, 9248–9259.
65. Shealy, R. T.; Murphy, A. D.; Ramarathnam, R.; Jakobsson, E.; Subramaniam, S. Sequence-Function Analysis of the K^+-Selective Family of Ion Channels Using a Comprehensive Alignment and the KcsA Channel Structure. *Biophys. J.* **2003**, *84*, 2929–2942.
66. Lenaeus, M. J.; Vamvouka, M.; Focia, P. J.; Gross, A. Structural Basis of TEA Blockade in a Model Potassium Channel. *Nat. Struct. Mol. Biol.* **2005**, *12*, 454–459.
67. Posson, D. J.; McCoy, J. G.; Nimigean, C. M. The Voltage-Dependent Gate in MthK Potassium Channels is Located at the Selectivity Filter. *Nat. Struct. Mol. Biol.* **2013**, *20*, 159–166.
68. Schneidman-Duhovny, D.; Inbar, Y.; Polak, V.; Shatsky, M.; Halperin, I.; Benyamini, H.; Barzilai, A.; Dror, O.; Haspel, N.; Nussinov, R.; *et al.* Taking Geometry to its Edge: Fast Unbound Rigid (and Hinge-Bent) Docking. *Proteins* **2003**, *52*, 107–112.
69. Zhang, C.; Vasmatzis, G.; Cornette, J. L.; DeLisi, C. Determination of Atomic Desolvation Energies from the Structures of Crystallized Proteins. *J. Mol. Biol.* **1997**, *267*, 707–726.
70. Andrusier, N.; Nussinov, R.; Wolfson, H. J. FireDock: Fast Interaction Refinement in Molecular Docking. *Proteins* **2007**, *69*, 139–159.
71. Kingsford, C. L.; Chazelle, B.; Singh, M. Solving and Analyzing Side-Chain Positioning Problems Using Linear and Integer Programming. *Bioinformatics* **2005**, *21*, 1028–1036.
72. Phillips, J. C.; Braun, R.; Wang, W.; Gumbart, J.; Tajkhorshid, E.; Villa, E.; Chipot, C.; Skeel, R. D.; Kalé, L.; Schulten, K. Scalable Molecular Dynamics with NAMD. *J. Comput. Chem.* **2005**, *26*, 1781–1802.
73. MacKerell, A. D.; Bashford, D.; Bellott, M.; Dunbrack, R. L.; Evanseck, J. D.; Field, M. J.; Fischer, S.; Gao, J.; Guo, H.; Ha, S.; *et al.* All-Atom Empirical Potential for Molecular Modeling and Dynamics Studies of Proteins. *J. Phys. Chem. B* **1998**, *102*, 3586–3616.
74. Jorgensen, W. L.; Chandresekhar, J.; Madura, J. D.; Impey, R. W.; Klein, M. L. Comparison of Simple Potential Functions for Simulating Liquid Water. *J. Chem. Phys.* **1983**, *79*, 926–935.
75. Essmann, U.; Perera, L.; Berkowitz, M. L.; Darden, T.; Lee, H.; Pedersen, L. G. A Smooth Particle Mesh Ewald Method. *J. Chem. Phys.* **1995**, *103*, 8577–8593.
76. Feller, S. E.; Zhang, Y. H.; Pastor, R. W.; Brooks, B. R. Constant-Pressure Molecular Dynamics Simulation: The Langevin Piston Method. *J. Chem. Phys.* **1995**, *103*, 4613–4621.
77. Martyna, G. J.; Tobias, D. J.; Klein, M. L. Constant Pressure Molecular Dynamics Algorithms. *J. Chem. Phys.* **1994**, *101*, 4177–4189.
78. Miyamoto, S.; Kollman, P. A. Settle—An Analytical Version of the Shake and Rattle Algorithm for Rigid Water Molecules. *J. Comput. Chem.* **1992**, *13*, 952–962.
79. Baker, N. A.; Sept, D.; Joseph, S.; Holst, M. J.; McCammon, J. A. Electrostatics of Nanosystems: Application to Microtubules and the Ribosome. *Proc. Natl. Acad. Sci. U. S. A.* **2001**, *98*, 10037–10041.
80. Torrie, G. M.; Valleau, J. P. Monte-Carlo Free-Energy Estimates Using Non-Booltzman Sampling—Application to Subcritical Lennard−Jones Fluid. *Chem. Phys. Lett.* **1974**, *28*, 578–581.
81. Kumar, S.; Bouzida, D.; Swendsen, R. H.; Kollman, P. A.; Rosenberg, J. M. The Weighted Histogram Analysis Method for Free-Energy Calculations on Biomolecules 0.1. The Method. *J. Comput. Chem.* **1992**, *13*, 1011–1021.